films were evaporated on the disk surfaces, yielding well-defined internal markers of fault offsets. All deformed specimens were observed by optical and scanning electron microscopy (SEM); all half-tone figures are back-scattered electron images taken at 20 kV acceleration voltage with a Philips XL-30 SEM with a field emission gun.

Received 17 November 2003; accepted 17 February 2004; doi:10.1038/nature02412.

1. Raleigh, C. B. & Paterson, M. S. Experimental deformation of serpentinite and its tectonic implications. *J. Geophys. Res.* **70,** 3965–3985 (1965).
2. Green, H. W. & Houston, H. The mechanics of deep earthquakes. *Annu. Rev. Earth Planet. Sci.* **23,** 169–213 (1995).
3. Kirby, S. Intraslab earthquakes and phase changes in subducting lithosphere. *Rev. Geophys.* **33**(suppl.), 287–297 (1995).
4. Wong, T.-F., Ko, S. C. & Olgaard, D. L. Generation and maintenance of pore pressure excess in a dehydrating system, 2. Theoretical analysis. *J. Geophys. Res.* **102,** 841–852 (1997).
5. Dobson, D. P., Meredith, P. G. & Boon, S. A. Simulation of subduction zone seismicity by dehydration of serpentine. *Science* **298,** 1407–1410 (2002).
6. Murrell, S. A. F. & Ismail, I. A. H. The effect of decomposition of hydrous minerals on the mechanical properties of rocks at high pressures and temperatures. *Tectonophysics* **31,** 207–258 (1976).
7. Rutter, E. H. & Brodie, K. H. Experimental "syntectonic" dehydration of serpentinite under conditions of controlled pore water pressure. *J. Geophys. Res.* **93,** 4907–4932 (1988).
8. Meade, C. & Jeanloz, R. Deep-focus earthquakes and recycling of water into the earth's mantle. *Science* **252,** 68–72 (1991).
9. Peacock, S. Are the lower planes of double seismic zones caused by serpentine dehydration in subducting oceanic mantle? *Geology* **29,** 299–302 (2001).
10. Seno, T., Zhao, D., Kobayashi, Y. & Nakamura, M. Dehydration of serpentinized slab mantle: seismic evidence from southwest Japan. *Earth Planets Space* **53,** 861–871 (2001).
11. Omori, S., Kamiya, S., Maruyama, S. & Zhao, D. Morphology of the intraslab seismic zone and devolatilization phase equilibria of the subducting slab peridotite. *Bull. Earthq. Res. Inst. Univ. Tokyo* **76,** 455–478 (2002).
12. Ulmer, P. & Trommsdorff, V. Serpentine stability to mantle depths and subduction related magmatism. *Science* **268,** 858–861 (1995).
13. Rispoli, R. Stress fields about strike-slip faults inferred from stylolites and tension gashes. *Tectonophysics* **75,** T29–T36 (1981).
14. Fletcher, R. C. & Pollard, D. D. Anticrack model for pressure solution surfaces. *Geology* **9,** 419–424 (1981).
15. Aydin, A. & Nur, A. Evolution of pull-apart basins and their scale independence. *Tectonics* **1,** 91–105 (1982).
16. Burnley, P. C. *The Effect of Nonhydrostatic Stress on the Olivine-spinel Transformation in Mg_2GeO_4.* Thesis, Univ. California, Davis (1990).
17. Bureau, H. & Keppler, H. Complete miscibility between silicate melts and hydrous fluids in the upper mantle: experimental evidence and geochemical implications. *Earth Planet. Sci. Lett.* **165,** 187–196 (1999).
18. Agee, C. B. & Walker, D. Static compression and olivine flotation in ultrabasic silicate liquid. *J. Geophys. Res.* **93,** 3437–3449 (1988).
19. Silver, P. G. *et al.* Rupture characteristics of the deep Bolivian earthquake of 1994 and the mechanism of deep-focus earthquakes. *Science* **268,** 69–73 (1995).
20. Hacker, B. R., Peacock, S. M., Abers, G. A. & Holloway, S. D. Subduction factory – 2. Are intermediate-depth earthquakes in subducting slabs linked to metamorphic dehydration reaction? *J. Geophys. Res. B* **108,** doi:10.1029/2001JB001129 (2003).
21. Jiao, W., Silver, P. G., Fei, Y. & Prewitt, C. T. Do intermediate- and deep focus earthquakes occur on preexisting weak zones? An examination of the Tonga subduction zone. *J. Geophys. Res.* **105,** 28125–28138 (2000).
22. Christova, C. & Scholz, C. H. Stresses in the Vanuatu subducting slab: A test of two hypotheses. *Geophys. Res. Lett.* **30,** doi:10.1029/2003GL017701 (2003).
23. Zhao, D., Mishra, O. P. & Sanda, R. Influence of fluids and magma on earthquakes: seismological evidence. *Phys. Earth. Planet. Inter.* **132,** 249–267 (2002).
24. Zhang, J., Green, H. W. II, Bozhilov, K. N. & Jin, Z.-M. Faulting induced by precipitation of water at grain boundaries in hot subducting oceanic crust. *Nature* (in the press).
25. Stalder, R. & Ulmer, P. Phase relations of a serpentine composition between 5 and 14 GPa: significance of clinohumite and phase E as water carriers into the transition zone. *Contrib. Mineral. Petrol.* **140,** 670–679 (2001).
26. Niu, F., Silver, P. G., Nadeau, R. M. & McEvilly, T. V. Migration of seismic scatterers associated with the 1993 Parkfield aseismic transient event. *Nature* **426,** 544–548 (2003).
27. Bromiley, G. D. & Pawley, A. R. The stability of antigorite in the systems MgO-SiO_2-H_2O (MSH) and MgO-Al_2O_3-SiO_2-H_2O (MASH): The effects of Al^{3+} substitution on high-pressure stability. *Am. Mineral.* **88,** 99–108 (2003).
28. Green, H. W. II & Borch, R. S. A new molten salt cell for precision stress measurement at high pressure. *Eur. J. Mineral.* **1,** 213–219 (1989).
29. Green, H. W., Young, T. E., Walker, D. & Scholz, C. H. Anticrack-associated faulting at very high-pressure in natural olivine. *Nature* **348,** 720–722 (1990).

Acknowledgements We thank V. Trommsdorff for sample material corresponding to that used in ref. 12; J. Zhang for discussions; K. Bozhilov for assistance with microscopy and photography; and F. Forgit for specimen assembly preparation and laboratory assistance. This work was supported by the US National Science Foundation.

Competing interests statement The authors declare that they have no competing financial interests.

Correspondence and requests for materials should be addressed to H.W.G. (hgreen@mail.ucr.edu).

The decline and fate of an iron-induced subarctic phytoplankton bloom

Philip W. Boyd[1], Cliff S. Law[2], C.S. Wong[3], Yukihiro Nojiri[4], Atsushi Tsuda[5], Maurice Levasseur[6], Shigenobu Takeda[7], Richard Rivkin[8], Paul J. Harrison[9,10], Robert Strzepek[11], Jim Gower[3], R. Mike McKay[12], Edward Abraham[2], Mike Arychuk[3], Janet Barwell-Clarke[3], William Crawford[3], David Crawford[3], Michelle Hale[8], Koh Harada[13], Keith Johnson[3], Hiroshi Kiyosawa[14], Isao Kudo[15], Adrian Marchetti[16], William Miller[17], Joe Needoba[9], Jun Nishioka[18], Hiroshi Ogawa[19], John Page[3], Marie Robert[3], Hiroaki Saito[20], Akash Sastri[21], Nelson Sherry[9], Tim Soutar[3], Nes Sutherland[3], Yosuke Taira[15], Frank Whitney[3], Shau-King Emmy Wong[3] & Takeshi Yoshimura[18]

[1]*NIWA Centre for Chemical and Physical Oceanography, Department of Chemistry, University of Otago, PO Box 56, Dunedin, 9003, New Zealand*
[2]*National Institute of Water and Atmospheric Research, 301 Evans Bay Parade, Greta Point, PO Box 14-901, Kilbirnie, Wellington, New Zealand*
[3]*Fisheries and Oceans Canada, Institute of Ocean Sciences, PO Box 6000, Sidney, British Columbia, V8L 4B2 Canada*
[4]*National Institute for Environmental Studies, Tsukuba, Ibaraki 305-8506, Japan*
[5]*Ocean Research Institute, University of Tokyo, Nakano, Tokyo 164-8639, Japan*
[6]*Department of Biology, University of Laval, Quebec, G1K 7P4, Canada*
[7]*Department of Aquatic Bioscience, University of Tokyo, Bunkyo, Tokyo 113-8657, Japan*
[8]*Ocean Sciences Centre, Memorial University of Newfoundland, St John's, Newfoundland, A1C 5S7, Canada*
[9]*Earth and Ocean Sciences, University of British Columbia, 6270 University Blvd, Vancouver, British Columbia, V6T 1Z4, Canada*
[10]*Hong Kong University of Science and Technology, Clear Water Bay, Hong Kong*
[11]*Department of Chemistry, University of Otago, PO Box 56, Dunedin, 9003, New Zealand*
[12]*Department of Biological Sciences, Bowling Green State University, Bowling Green, Ohio 43403, USA*
[13]*National Institute of Advanced Industrial Science and Technology, 1-3-1, Kasumigaseki, Chiyoda-ku, Tokyo 100-8921, Japan*
[14]*Marine Biological Research Institute of Japan, Shinagawa, Tokyo 142-0042, Japan*
[15]*Graduate School of Fisheries Science, Hokkaido University, Hakodate, Hokkaido 041-8611, Japan*
[16]*Department of Botany, University of British Columbia, 6270 University Blvd, Vancouver, British Columbia, V6T 1Z4, Canada*
[17]*Dalhousie University, Department of Oceanography, Halifax, Nova Scotia, B3H 4J1 Canada*
[18]*Central Research Institute of Electric Power Industry, Abiko, Chiba 270-1194, Japan*
[19]*Marine Biogeochemistry Laboratory, Ocean Research Institute, The University of Tokyo 1-15-1, Minamidai, Nakano, Tokyo 164-8639, Japan*
[20]*Tohoku National Fisheries Research Institute, Shiogama, Miyagi 985-0001, Japan*
[21]*School of Earth and Ocean Sciences, University of Victoria, Victoria, British Columbia, V8W 3N5, Canada*

Iron supply has a key role in stimulating phytoplankton blooms in high-nitrate low-chlorophyll oceanic waters[1–5]. However, the fate of the carbon fixed by these blooms, and how efficiently it is exported into the ocean's interior, remains largely unknown[1–5]. Here we report on the decline and fate of an iron-stimulated diatom bloom in the Gulf of Alaska. The bloom terminated on day 18, following the depletion of iron and then silicic acid, after which mixed-layer particulate organic carbon (POC) concentrations declined over six days. Increased particulate silica export via sinking diatoms was recorded in sediment traps at depths between 50 and 125 m from day 21, yet increased POC export was not evident until day 24. Only a small proportion of the

mixed-layer POC was intercepted by the traps, with more than half of the mixed-layer POC deficit attributable to bacterial remineralization and mesozooplankton grazing. The depletion of silicic acid and the inefficient transfer of iron-increased POC below the permanent thermocline have major implications both for the biogeochemical interpretation of times of greater iron supply in the geological past[6,7], and also for proposed geoengineering schemes to increase oceanic carbon sequestration[3,8].

The magnitude of iron supply to the oceans has changed over geological timescales[6,9], and the increased export of carbon from iron-stimulated phytoplankton blooms is one of several mechanisms proposed for past reductions in atmospheric CO_2 concentrations[6]. Mesoscale *in situ* iron enrichments have resulted in diatom blooms, demonstrating that phytoplankton growth in high-nitrate low-chlorophyll (HNLC) waters is controlled by the iron supply[1–5]. The deliberate iron enrichment of HNLC regions has therefore been considered as a potential strategy to mitigate the current rise in atmospheric CO_2 (refs 3 and 8). However, mesoscale iron enrichments have not studied the decline of a bloom [1–5], or quantified the associated POC export[1–5].

During the subarctic ecosystem response to iron enrichment study (SERIES), we made the first comprehensive time-series measurements of the decline and fate of an iron-induced diatom bloom. During the bloom decline, the mixed-layer POC inventory decreased by 258 mmol m^{-2}, yet only 18% of this POC was exported to a depth of 50 m, with 8% being detected below the permanent thermocline (~120 m, ref. 10). We can account for at least 69% of this decrease in iron-elevated mixed-layer POC, with the majority due to bacterial remineralization both within and below the mixed layer.

An initial survey on 7 and 8 July 2002 located a site northeast of Ocean Station Papa (OSP, 50° N, 145° W), in the Gulf of Alaska, with HNLC characteristics typical of this region[10–12]. On 9 July 2002, a 77 km^2 patch of HNLC waters was enriched with sulphur hexafluoride (SF_6) (>400 fmol l^{-1}) and dissolved iron (>1 nmol l^{-1}, Fig. 1a). SERIES commenced on 10 July 2002 (day 0), and concluded on 4 August 2002 (day 25). On day 6, a second iron infusion (without SF_6 tracer) raised the dissolved iron to 0.6 nmol l^{-1} (Fig. 1a). The patch of iron-enriched waters stretched into an ellipsoid along a north–south axis, increased in area to >200 km^2 by day 13, and to a maximum of ~1,000 km^2 by days 17/18, at which time a 70–80 μatm drawdown of CO_2 was evident (Supplementary Fig. 1a).

The development of an iron-stimulated bloom was evident from increases in chlorophyll to ~5 mg m^{-3} (Fig. 1b), with a corresponding increase in POC and particulate silica (PSi) concentrations (Fig. 1c). Diatom biomass was initially low, increased exponentially (Fig. 1b), and then decreased around day 18 corresponding to the decline in chlorophyll concentrations (Fig. 1b). The onset of algal iron limitation occurred around day 12, after which photosynthetic competence (F_v/F_m) progressively decreased to the levels observed in the surrounding waters (Supplementary Fig. 1b). The dissolved iron decreased to HNLC concentrations[11] by day 12 (Fig. 1a), followed by silicic acid depletion to <2 mmol m^{-3} by day 16 (Fig. 1d), despite the re-supply of silicic acid via lateral entrainment of surrounding waters (see Methods). Microzooplankton grazing mortality on phytoplankton of <202 μm was initially 0.42 d^{-1}, then decreased to 0.09 d^{-1} by day 6 and remained constant during the bloom evolution (compare with algal growth rates of up to 0.45 d^{-1} on day 13, data not shown). Mesozooplankton herbivory was highest during the bloom decline (10.8 mmol of carbon per m^2 per day, compared with 6.0 mmol C m^{-2} d^{-1} in the surrounding waters) with daily rates equivalent to 2% of the POC inventory on day 18 (Fig. 1c). Thus, bloom termination was driven by resource limitation, rather than top-down control[13].

The decline of the bloom was signalled by rapid decreases in POC and PSi concentrations at the patch centre after day 18 (Fig. 1c) with 75–79% deficits in surface mixed layer inventories by day 25 (Table 1). The bloom decline was also evident from space, with sea-viewing wide field of view sensor (SeaWiFS) images providing

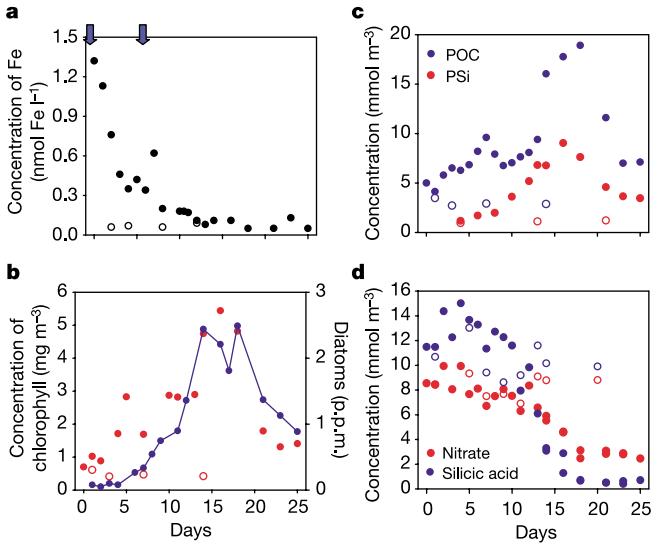

Figure 1 Time series of 'In' (patch centre, solid symbols) and 'Out' (surrounding waters, open symbols) mean mixed layer properties. **a**, Dissolved iron, arrows denote iron infusions. **b**, Chlorophyll (red) and diatom biovolume[14] (blue, 5 m depth). **c**, POC (blue) and PSi (red). **d**, Nitrate (red, 5 m) and silicic acid (blue, 5 m). The standard error ($n = 3$) was: <0.02 nmol l^{-1} for dissolved iron; smaller than the symbols for nitrate and silicic acid; <0.1 below 1 mg chl m^{-3}, and <0.3 for chlorophyll between 1 and 5 mg m^{-3}. POC data were derived from 1 m resolved transmissivity profiles and a POC algorithm[27] (see Methods).

Table 1 **Upper ocean budgets of biogenic particles at the patch centre**

Parameter	Depth (m)	POC (mmol m^{-2})	PSi (mmol m^{-2})
Accumulation until day 18	0–25	328	200
Inventory on day 25	0–25	70	51
Mixed layer deficit of POC days 18–23	0–25	−258	−149
Fate of mixed-layer POC deficit			
Export flux	at 50	−47 (18%)	−51 (34%)
Undertrapping*	at 50	−11	
Mesozooplankton herbivory†	0–30	−29	
Remineralization to DIC‡	10–30	−90	
Differential remineralization of PSi and POC from trap§	0–50	−41	
PSi dissolution‖	10–30	−128	
Remineralization based on NH_4 accumulation¶	0–25	−100	

Water column inventories and fluxes are defined as ('In' minus 'Out'). Loss terms are assigned a negative sign. Between 69% and 99% of the observed mixed layer POC deficit was accounted for. Export efficiency is reported as a percentage, and defined as: (POC export/POC deficit) × 100. For this export calculation, inventories were not corrected for dilution because the patch size was greater (200–1,000 km^2) than the source square (for mixed-layer particles intercepted at depth, 50–200 km^2)[30] throughout. DOC concentrations changed little between days 18 and 23 and ranged from 1.27 ± 0.03 to 1.34 ± 0.03 mol m^{-2} in the patch (0–20 m integrals). Microzooplankton herbivory was not included as a POC loss term because there are no data after day 17. We did not consider data on carbon losses before day 18 because during this period there were no significant differences in the magnitude of loss terms between 'In' and 'Out' waters.

*Potential particle flux (24%) not intercepted by the traps based on a radiochemical trap calibration (see Methods).

†Estimate based on the mean of five grazing experiments on days 18, 19, 20, 22 and 23. The standard error of the mean was 0.6 mmol m^{-2} d^{-1}.

‡Derived from increases in the DIC inventory between days 18 and 23 only (Fig. 2c).

§Derived from bacterially mediated differential remineralization of PSi relative to POC[16] at 50 m, and equivalent to a POC loss of 41 mmol m^{-2} ((34% minus 18%) × 258 mmol C m^{-2}).

‖Calculated from excess silicic acid observed between days 18 and 23. Variability in silicic acid concentrations below 30 m precludes an estimate of DIC changes at depth. Remineralization estimates based on PSi and silicic acid of 169 mmol C m^{-2} (128 + 41) are higher than that derived from DIC increases (90 mmol C m^{-2}), and give a POC loss of 99% (128 + 41 + 29 + 11 + 47).

¶Derived from a 15.1 mmol N m^{-2} accumulation of ammonium between days 18 and 23, converted to units of carbon using a Redfield C:N ratio of 6.6.

estimates of bloom areal extent, and homogeneity of algal biomass across the patch (Supplementary Fig. 2). During this decline phase, there were changes in downward particle fluxes (see Methods) below the patch ('In') at 50 to 125 m depth (Fig. 2a, b). Particle fluxes in the surrounding waters ('Out') were relatively constant at 50 m (see Methods), and the 'Out' and 'In' particle fluxes were similar at 50 m from days 1 to 18 (Fig. 2a, b). However, between days 18 and 21, particle abundances intercepted by 50 m 'In' traps increased eightfold, and were dominated both numerically (7:1) and volumetrically (3:1)[14,15] by diatom cells and aggregates compared with mesozooplankton faecal pellets. From day 21 onwards, 'In' particle fluxes exceeded those for 'Out' traps, with a threefold increase in PSi flux at 50 m depth (Fig. 2a). This trend was also observed for the deeper traps. In contrast to PSi fluxes, POC fluxes at 50 m rose marginally between days 21 and 23 (Fig. 2b), but then increased to 40 mmol $m^{-2} d^{-1}$ on day 24.5, and were elevated at greater depth (Fig. 2b).

The mixed-layer POC inventory declined by 79% (Table 1), as a result of vertical export (Fig. 2a, b), bacterial solubilization[16,17], and ingestion by grazers[18] both within and below the mixed layer. Decreases in mixed-layer POC were not due to physical factors such as vertical advection (Supplementary Fig. 3), or dilution arising from lateral spreading (Supplementary Fig. 2). Only 18% of the decrease in mixed-layer POC was subsequently intercepted by the 50 m trap (Table 1), although the trap may not have captured all of the settling particles[19]. Radiochemical calibration of a trap array identical to that deployed in SERIES (see Methods) indicates that these traps potentially undersampled export flux by up to 24% (Table 1), signifying that a maximum 22% of the mixed-layer POC deficit could reach 50 m. Mesozooplankton herbivory of 4.8 mmol C $m^{-2} d^{-1}$ (see Methods) over six days accounted for 10% of the POC decline (Table 1). Between days 21 and 25, bacterial production rates of 0.3–0.4 mmol C $m^{-3} d^{-1}$ (upper 6 m only, see Methods) in the patch were double that measured on day 14, and three- to fourfold greater than in the surrounding waters. We used three indirect approaches to estimate bacterial remineralization of particles: changes in dissolved inorganic carbon (DIC) concentrations, selective preservation of opal, and ammonium accumulation (see Methods).

During the decline of the bloom between days 18 and 23, bacterial remineralization of particles[17] was responsible for increased DIC concentrations at depths of 10–30 m (that is, within and below the mixed layer, Fig. 2c), corresponding to concurrent decreases in POC within this depth horizon (Fig. 2d). This increase in DIC was equivalent to ~35% of the mixed-layer POC deficit (Table 1). Bacterial remineralization of POC was also inferred from selective preservation of PSi relative to POC[16,20] in the trap samples from 50 m depth (Table 1). Laboratory radiotracer experiments examining remineralization of diatom detritus have shown that POC is used considerably faster than PSi over a timescale of 4–6 days[16]. We used the PSi intercepted by the 50 m trap to calculate the additional amount of POC remineralized between 0 and 50 m (Table 1). Note that this is a lower bound, because some dissolution of PSi will have occurred in the overlying waters, as was confirmed by an increase in silicic acid of 51 mmol m^{-2} between days 18 and 23 over the 10–30 m horizon coincident with the DIC increase (Fig. 2c). POC remineralization is a precursor of PSi dissolution[20], so this increase in silicic acid is equivalent to a DIC increase of 128 mmol m^{-2} (using a mixed layer PSi:POC molar ratio of 0.4, data not shown). The ammonium accumulation in the upper 25 m of the patch

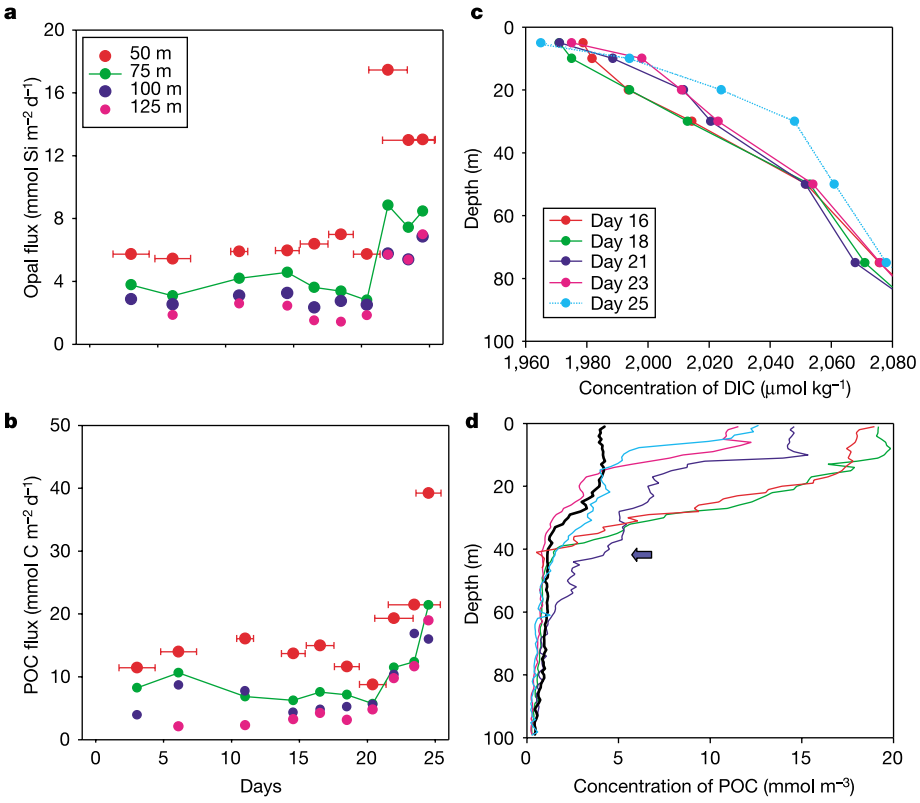

Figure 2 Export and remineralization at the patch centre during the bloom decline. **a,** Downward opal flux intercepted by trap arrays. Symbols denote the deployment midpoint, and horizontal bars the deployment timescales. **b**, POC fluxes from the corresponding deployments as in **a**. **c**, DIC profiles. Standard error bars were always smaller than symbols. Changes in DIC were not assessed after day 23 owing to the intrusion of denser waters (20–50 m) (Supplementary Fig. 3). **d**, POC profiles for the patch centre[27]. Colour-coding as in **c**, the black profile represents an 'Out' station (day 14). The arrow denotes sinking and/or stationary particles between 35 and 50 m on day 21.

Table 2 **Calculated Fe:C molar ratios during the SERIES bloom**

	Fe:C	Fe:C ratio	Data source
Added Fe:carbon fixation*	41.3 μmol:1.61 ± 0.12 mol	2.6×10^{-5} ($\pm 1.9 \times 10^{-6}$) mol mol^{-1}	Patch centre
Added Fe:POC accumulation†	2.43 tonnes $FeSO_4.7H_2O$: 1,776 ± 442 tonnes POC	$7.9 \times 10^{-5} \pm 2.0 \times 10^{-5}$	Entire patch†
Added Fe:POC export (50 m)‡	41.3 μmol:0.05 mol	8.3×10^{-4} mol mol^{-1}	Export signal is integrated over 50–200 km^2‡
Added Fe:POC export (125 m)‡	41.3 μmol:0.02 mol	2.1×10^{-3} mol mol^{-1}	Export signal is integrated over 50–200 km^2‡

The carbon fixation estimate takes into account dilution of the patch, that is, it includes all algal carbon fixation supported by iron enrichment (see Methods). Total iron added during two infusions was 41.3 μmol Fe m^{-2} (patch-centre concentrations were raised by 2.25 μmol Fe m^{-3} over 0–15 m (measured 16 h after the iron enrichment began), and by 0.3 μmol Fe m^{-3} over 0–25 m (day 6).
*Based on iron-mediated increases in net primary production of 1.61 ± 0.12 mol C m^{-2}. Increases in net primary production were greater than decreases in DIC estimated from a carbon budget of the patch centre (1.1 ± 0.07 mol C m^{-2}, see Methods), due in part to remineralization of POC to DIC (see Fig. 2c).
†Denotes an estimate of POC accumulation based on mean ± standard deviation of chlorophyll from the SeaWiFS Ocean Colour image on day 19 (Supplementary Fig. 3) multiplied by the carbon:chlorophyll ratio for day 18 at the patch centre (80 g:g) and a mixed layer depth of 25 m.
‡Denotes the range of calculated source-squares (using current speed and algal sinking rate data) for mixed-layer particles that are intercepted at depth by sediment traps[30].

between days 18 and 23 was equivalent to a DIC increase of 100 mmol m^{-2}, in good agreement with the other two indirect methods. Taken together, loss processes and a sampling artefact account for 69% (based on DIC) to 99% (based on PSi) of the fivefold decrease in mixed-layer POC, with bacterial remineralization accounting for the greatest proportion of the decrease (Table 1).

The bloom was initiated within a SF_6-labelled control volume, enabling the construction of a carbon budget for the patch centre (corrected for dilution, see Methods) to provide estimates of Fe:C stoichiometry[3,8]. The ratio of Fe:C fixed for the patch centre (2.6×10^{-5}, Table 2), is higher than those ($2 \times 10^{-6} - 7 \times 10^{-6}$) derived from laboratory cultures[21]. Although this ratio was computed for the patch centre, we extrapolated to a Fe:POC accumulation ratio of 7.9×10^{-5} for the entire patch. Budgets and trap data reveal that the vertical transfer efficiency of POC was 18% between the mixed layer and 50 m (Table 1), increasing to ~50% at depths of 50–125 m (Fig. 2b). As with surface waters (Table 1), it is likely that bacterial remineralization[17] was the main process responsible for the attenuation of the bloom export signal below 50 m. Owing to this inefficient vertical transfer of POC from the mixed layer to 125 m (8%; 21 mmol C m^{-2}:258 mmol C m^{-2}), the ratios for Fe:C export to depth were substantially higher than those for the mixed layer (Table 2). Although a further 23% of mixed-layer iron-elevated POC remained in the surface waters on day 25 (Table 1), the SERIES 'export efficiency' of 8% in our labelled patch is low compared with naturally occurring open-ocean blooms (15–30%, ref. 22) which were sampled in eulerian mode.

SERIES has provided the first detailed evaluation of the decline and fate of an iron-stimulated bloom. Our findings show that although bloom dynamics are controlled by iron supply, bloom termination is also influenced by silicic acid availability. The observed depletion of silicic acid is in contrast to results from modelling simulations of iron-stimulated diatom blooms in the glacial Southern Ocean[7]. Furthermore, silicic acid depletion indicates that an increased iron supply, as occurred during the glacial periods[6,9], may not have been the only prerequisite to sustain blooms of siliceous algae. Our study indicates that a concurrent supply of silicic acid would be required for iron-stimulated diatom blooms to persist; this possibility has been reported from the geological record[23]. The added Fe:C exported below the permanent thermocline near OSP of 2.1×10^{-3} is a thousandfold higher than that used by geo-engineers to assess the efficiency and cost-effectiveness of iron enrichment as a strategy for mitigating the effects of climate change[3,8]. Proposed schemes for oceanic iron fertilization to ameliorate anthropogenic increases in atmospheric CO_2 have advocated a strategy of repeated iron enrichments[3,8]. Our results indicate that the influence of silicic acid depletion may negate the impact of such repeated iron enrichment on diatom stocks, and moreover that inefficient vertical transfer of carbon may limit the effectiveness of iron fertilization as a mitigation strategy. □

Methods

Iron/SF_6 release and mapping

Concurrent addition of acidified dissolved iron (ferrous sulphate, pH 2)[2] and SF_6 at 7 m depth followed an expanding square pattern over 4.75 × 4.74 nautical miles, that was modified for lagrangian drift using an uplink radio-buoy[24]. The drogued ARGOS-GPS drifter buoy at the patch centre subsequently assisted our daily mapping of the patch[24]. On day 6, a successful iron re-infusion took place in an expanding rectangle of 7.3 by 3.7 nautical miles. As SF_6 reinfusion was not required, mapping allowed real-time discrimination of the patch centre during reinfusion, with cessation of iron supply when the concentration of SF_6 reached <25 fmol l^{-1}.

Correction for entrainment

Temporal changes in concentrations of properties at the patch centre were driven by bloom dynamics, but were influenced concurrently by lateral entrainment of the surrounding waters, causing dilution or supplementation depending on the concentration gradients. Thus, gradients from high concentrations at the patch centre to low concentrations in 'Out' waters (such as POC) resulted in dilution of POC at the patch centre. The reverse concentration gradient (such as for DIC) maintained lateral supply of DIC to the patch centre from surrounding waters. These additional supply/loss terms were accounted for in a carbon budget, by estimating the strain rate of the SF_6-labelled patch[25] for days 1–13, and applying the resulting entrainment factor to the 'In'–'Out' gradient for each property. Shipboard incubations, including primary production, were not subject to entrainment effects, and so were not corrected.

Carbon budget

To obtain estimates of carbon fixed per unit iron added, a budget was constructed on the basis of cumulative changes in net primary production (NPP) and DIC concentrations until day 20. Changes in concentrations (or rates) were obtained from 'In' minus 'Out' values for the period when 'In' values exceeded the corresponding 'Out' values (or vice versa for DIC), resulting in each term being summed over slightly different time periods.

Vertical sampling

Sampling took place at the patch centre as defined by daily SF_6 mapping, and water was obtained for fast-repetition-rate fluorometry (FRRF) (ref. 2) (Supplementary Fig. 2), PSi (ref. 26), DIC (ref. 2) and dissolved iron, using a clean vertical pumping system[11]. All 'Out' stations (>20 km northeast of the patch) were characterized by background SF_6 concentrations. POC data were obtained from an algorithm validated in waters exhibiting a wide range of primary productivity including HNLC (OSP) and mesotrophic waters[27], and initial POC concentrations were comparable to those at OSP[27]. A limited number of mixed-layer POC measurements were available and agreed closely with those from the algorithm[27]. POC replicates were not available, but seven POC profiles from the patch centre (day 23) exhibited ~7% variation. No replicates for PSi were available. Mesozooplankton herbivory was estimated by the gut pigment technique[28] in conjunction with gut evacuation rates[28] and carbon:chlorophyll ratios from corresponding days. Key properties, including macronutrients and F_v/F_m, were measured on at least two vessels. Whenever possible identical protocols were used (for example, FRRF). Successful intercalibrations (that is ±10–15%) were performed before (for example, dissolved iron) or during SERIES (for example, macronutrients).

Trap deployments and trapping efficiency

Particle export fluxes were derived from surface-tethered free-drifting traps for 'In' and 'Out' waters at depths of 50 m, 75 m, 100 m and 125 m for 1.8–3.8-day intervals, with overlap between some deployments and recoveries. The 50 m 'Out' opal fluxes were 6.3, 4.8 and 5.3 mmol m^{-2} d^{-1} for deployments centred on days 3, 6 and 15, respectively. The 50-m 'Out' POC fluxes were 16.0, 8.9, 11.6 mmol m^{-2} d^{-1} for days 3, 6 and 15, respectively. Calibration of the trapping efficiency using ^{234}Th (ref. 19), of an identical trap array to that used in SERIES, were undertaken in the northwest Pacific at time series station KNOT[26]. Two calibrations (May 1999) indicated that trapping efficiency was ~76% at 150 m (by comparing ^{234}Th flux from the vertical profile of ~1,330 d.p.m. m^{-2} d^{-1} with ~1,030 d.p.m. m^{-2} d^{-1} from traps, where d.p.m. is decays per minute). Trapping efficiencies were >90% at depths of 80–120 m, and at 50 m were in some cases >100%. So a worst-case scenario assumes 24% undertrapping of particles by our traps. The May 1999 trap calibration is applicable as it was conducted in waters with diatom-dominated particle fluxes[26], beneath a 30 m mixed layer, and with upper-ocean

currents of $<20\,cm\,s^{-1}$, as observed during SERIES. Trapping efficiency is thought to be determined by the characteristics of sinking particles, trap design and upper-ocean hydrodynamics[19]. The location of the 'In' traps relative to the patch was monitored using a logging fluorometer 10 m subsurface on the surface-tethered array. Traps remained near the patch centre; on day 23 the array was at the periphery for 36 h before recovery and therefore underestimated vertical export. 'Out' traps were deployed at least 20 km northeast of the patch. Limited replicates were available from trap cups, and the standard error ($n = 3$) for fluxes was ± 1.3 mmol Si $m^{-2}\,d^{-1}$ and ± 2.5 mmol C $m^{-2}\,d^{-1}$ for the 75 and 100 m 'In' traps on day 14.

Bacterial remineralization of particles

We had no information on bacterial growth efficiency, which was required to calculate bacterial carbon demand[29]: demand = bacterial production × (1/growth efficiency), published values display a range from 0.1 to 0.7 (ref. 29). Therefore, we employed indirect approaches (changes in DIC concentrations, selective preservation of opal and ammonium accumulation) to estimate particle remineralization.

Received 16 November 2003; accepted 24 February 2004; doi:10.1038/nature02437.
Published online 17 March 2004.

1. Coale, K. H. *et al.* A massive phytoplankton bloom induced by an ecosystem-scale iron fertilization experiment in the equatorial Pacific Ocean. *Nature* **383,** 495–501 (1996).
2. Boyd, P. W. *et al.* A mesoscale phytoplankton bloom in the polar Southern Ocean stimulated by iron fertilization. *Nature* **407,** 695–702 (2000).
3. Buesseler, K. O. & Boyd, P. W. Will ocean fertilization work? *Science* **300,** 67–68 (2003).
4. Gervais, F., Riebesell, U. & Gorbunov, M. Y. Changes in primary productivity and chlorophyll *a* in response to iron fertilization in the Southern Polar Frontal Zone. *Limnol. Oceanogr.* **47,** 1324–1335 (2002).
5. Tsuda, A. *et al.* A mesoscale iron enrichment in the western Subarctic Pacific induces a large centric diatom bloom. *Science* **300,** 958–961 (2003).
6. Martin, J. H. Glacial-interglacial CO_2 change: The iron hypothesis. *Paleoceanography* **5,** 1–13 (1990).
7. Matsumoto, K., Sarmiento, J. L. & Brzezinski, M. A. Silicic acid leakage from the Southern Ocean: A possible explanation for glacial atmospheric pCO_2. *Glob. Biogeochem. Cycles* **16,** doi:10.1029/2001GB001442 (2002).
8. Chisholm, S. W., Falkowski, P. G. & Cullen, J. J. Oceans—Discrediting ocean fertilization. *Science* **294,** 309–310 (2001).
9. Petit, J. R. *et al.* Climate and atmospheric history of the past 420,000 years from the Vostok ice core, Antarctica. *Nature* **399,** 429–436 (1999).
10. Tabata, S. The general circulation of the Pacific Ocean and a brief account of the oceanographic structure of the North Pacific Ocean. Part I—Circulation and volume transports. *Atmosphere* **13,** 133–168 (1975).
11. Nishioka, J., Takeda, S., Wong, C. S. & Johnson, W. K. Size-fractionated iron concentrations in the northeast Pacific Ocean: distribution of soluble and small colloidal iron. *Mar. Chem.* **74,** 157–179 (2001).
12. LaRoche, J., Boyd, P. W., McKay, R. M. L. & Geider, R. J. Flavodoxin as an *in situ* marker for iron stress in phytoplankton. *Nature* **382,** 802–805 (1996).
13. Cullen, J. J. Hypothesis to explain high-nutrient conditions in the open sea. *Limnol. Oceanogr.* **36,** 1578–1599 (1991).
14. Strathmann, R. R. Estimating the organic carbon content of phytoplankton from cell volume or plasma volume. *Limnol. Oceanogr.* **12,** 411–418 (1967).
15. Komar, P. D., Morse, A. P., Small, L. F. & Fowler, S. W. An analysis of sinking rates of natural copepod and euphausiid fecal pellets. *Limnol. Oceanogr.* **26,** 172–180 (1981).
16. Bidle, K. D., Manganelli, M. & Azam, F. Regulation of oceanic silicon and carbon preservation by temperature control on bacteria. *Science* **298,** 1980–1984 (2002).
17. Smith, D. C., Simon, M., Alldredge, A. L. & Azam, F. Intense hydrolytic enzyme activity on marine aggregates and implications for rapid particle dissolution. *Nature* **359,** 139–142 (1992).
18. Dagg, M. Sinking particles as a possible source of nutrition for the large calanoid copepod *Neocalanus cristatus* in the sub-arctic Pacific Ocean. *Deep-Sea Res. I* **40,** 1431–1445 (1993).
19. Buesseler, K. O., Michaels, A. F., Siegel, D. A. & Knap, A. H. A 3-dimensional time-dependent approach to calibrating sediment trap fluxes. *Glob. Biogeochem. Cycles* **8,** 179–193 (1994).
20. Treguer, P. *et al.* The silica balance in the world ocean: a re-estimate. *Science* **268,** 375–379 (1995).
21. Sunda, W. G. & Huntsman, S. A. Iron uptake and growth limitation in oceanic and coastal phytoplankton. *Mar. Chem.* **50,** 189–206 (1995).
22. Buesseler, K. O. The decoupling of production and particulate export in the surface ocean. *Glob. Biogeochem. Cycles* **12,** 297–310 (1998).
23. Harrison, K. G. Role of increased marine silica input on paleo-pCO_2 levels. *Paleoceanography* **15,** 292–298 (2000).
24. Law, C. S., Abraham, E. R., Watson, A. J. & Liddicoat, M. Vertical diffusion and nutrient supply to the surface mixed layer of the Antarctic Circumpolar Current. *J. Geophys. Res.* **108,** doi:10.1029/2002JC001604 (2003).
25. Abraham, E. R. *et al.* Importance of stirring in the development of an iron-fertilized phytoplankton bloom. *Nature* **407,** 727–730 (2000).
26. Honda, M. C. *et al.* The biological pump in the northwestern North Pacific based on fluxes and major components of particulate matter obtained by sediment-trap experiments (1997–2000). *Deep-Sea Res. II* **49,** 5595–5625 (2002).
27. Bishop, J. K. B. Transmissiometer measurement of POC. *Deep-Sea Res. I* **46,** 353–369 (1999).
28. Tsuda, A. & Sugisaki, H. In-situ grazing rate of the copepod population in the western subarctic North Pacific during spring. *Mar. Biol.* **120,** 203–210 (1994).
29. Rivkin, R. & Legendre, L. Biogenic carbon cycling in the upper ocean: effects of microbial respiration. *Science* **291,** 2398–2400 (2001).
30. Siegel, D. A., Granata, T. C., Michaels, A. F. & Dickey, T. D. Mesoscale eddy diffusion, particle sinking, and the interpretation of sediment trap data. *J. Geophys. Res.* **95,** 5305–5311 (1990).

Supplementary Information accompanies the paper on **www.nature.com/nature.**

Acknowledgements We thank the officers and crews and scientists on board the *John P. Tully, El Puma* and *Kaiyo Maru*. We are grateful to S. Toews for shoreside logistical support. The manuscript was improved by comments from K. Currie, R. Frew, C. Hurd, P. Boyd, D. Hutchins and T. Trull. This study was supported by NSERC Canada as part of the C-SOLAS programme, CFCAS, DFO PERD (Canada), the New Zealand PGSF (Ocean Ecosystems), and the Global Environmental Research Fund from the Ministry of Environment, the Fisheries Agency, and the Central Research Institute of Electric Power Industry research funding (Japan).

Competing interests statement The authors declare that they have no competing financial interests.

Correspondence and requests for materials should be addressed to P.W.B. (p.boyd@niwa.co.nz).

Ferns diversified in the shadow of angiosperms

Harald Schneider[1,2], Eric Schuettpelz[1], Kathleen M. Pryer[1], Raymond Cranfill[3], Susana Magallón[4] & Richard Lupia[5,6]

[1]*Department of Biology, Duke University, Durham, North Carolina 27708, USA*
[2]*Albrecht-von-Haller-Institut für Pflanzenwissenschaften, Abteilung Systematische Botanik, Georg-August-Universität, Untere Karspüle 2, 37073 Göttingen, Germany*
[3]*University Herbarium, University of California, 1001 Valley Life Sciences Building #2465, Berkeley, California 94720, USA*
[4]*Departamento de Botánica, Instituto de Biología, Universidad Nacional Autónoma de México, Circuito Exterior, Anexo al Jardín Botánico, AP 70-233, México DF 04510, Mexico*
[5]*Sam Noble Oklahoma Museum of Natural History and*
[6]*School of Geology and Geophysics, University of Oklahoma, Norman, Oklahoma 73072, USA*

The rise of angiosperms during the Cretaceous period is often portrayed as coincident with a dramatic drop in the diversity and abundance of many seed-free vascular plant lineages, including ferns[1–5]. This has led to the widespread belief that ferns, once a principal component of terrestrial ecosystems[6], succumbed to the ecological predominance of angiosperms and are mostly evolutionary holdovers from the late Palaeozoic/early Mesozoic era. The first appearance of many modern fern genera in the early Tertiary fossil record implies another evolutionary scenario; that is, that the majority of living ferns resulted from a more recent diversification[7–10]. But a full understanding of trends in fern diversification and evolution using only palaeobotanical evidence is hindered by the poor taxonomic resolution of the fern fossil record in the Cretaceous[11]. Here we report divergence time estimates for ferns and angiosperms based on molecular data, with constraints from a reassessment of the fossil record. We show that polypod ferns (>80% of living fern species) diversified in the Cretaceous, after angiosperms, suggesting perhaps an ecological opportunistic response to the diversification of angiosperms, as angiosperms came to dominate terrestrial ecosystems.

The extraordinary diversification of angiosperms throughout the Cretaceous and Tertiary, culminating in an estimated 250,000–300,000 living species[3], is well known[1–4,12] owing to the exceptional fossil record of this lineage. The oldest fossils (Early Cretaceous) that can be unequivocally assigned to specific clades of angiosperms[3,12,13] correspond to the initially diverging lineages resolved in DNA-based phylogenetic analyses[14–16]. The well-sampled fossil record of subsequently derived angiosperms is also broadly congruent with phylogenetic analyses[12,14–16]. Ferns, with more than 10,000 living species, are the second largest group of vascular plants[7]. They attained remarkable levels of diversity and abundance from the Carboniferous to the Jurassic—a richness that is well